Numerical investigation on vortex-induced motions of a buoyancy can

Kangdi Xie, Weiwen Zhao, Decheng Wan*

Collaborative Innovation Center for Advanced Ship and Deep-Sea Exploration, State Key Laboratory of Ocean Engineering, School of Naval Architecture, Ocean and Civil Engineering, Shanghai Jiao Tong University, Shanghai, China

*Corresponding author: dcwan@sjtu.edu.cn

ABSTRACT

This paper presents three-dimensional (3D) Computational Fluid Dynamic (CFD) simulation to analyse the flow induced response (FIR) especially the yaw motion of a Buoyancy Can. The numerical cases are conducted with a Buoyancy Can under different reduced velocities utilizing naoe-FOAM-SJTU, a solver based on the open source toolkit OpenFOAM. SST-DDES model is applied to handle the flow separation, and oversets grid method is utilized to solve a large amplitude 6-Degrees-Of-Freedom (6-DOF) motions. Free decay test and vortex-induced motion (VIM) test are built numerically. In VIM cases, the responses of trajectory, amplitude, frequency are calculated in a series of reduced velocities. With the increase of reduced velocity, yaw frequency is increased, which is similar with surge and sway frequency. And yaw frequency is equal to the sway frequency, which is consistent with Kang's experimental results [1,2]. Furthermore, comparing two cases, one fixed in rotation and the other one free in rotation, we can obtain a conclusion that release in the degree of rotation can decrease the sway amplitude but make no difference in the surge amplitude.

1 INTRODUCTION

Buoyancy Cans in typical cylindrical shape are widely applied in deep water fields to tension a riser and keep it vertical [3] Flow over a Buoyancy Can induces an alternating vortex shedding, which causes in surge, sway and yaw motions. Recently studies concentrate on the motion characteristics of Spar platforms and semi-submersible platforms, while few researcher push forward the investigation in the VIM phenomenon especially the yaw motion of typical cylindrical object. Therefore, the buoyancy can in typical cylindrical shape is a suitable object to reveal the mechanical of VIM phenomenon.

Methods in investigating the VIM phenomenon can be normally divided into two categories, model test and numerical simulation. And a lot of model tests [4-5] to comprehend the mechanism of VIM have been delivered. Govardhan et al. (1997) [6] deliver a model test of a tethered sphere to investigate the VIM phenomenon. And they find that the tether sphere oscillates vigorously in a large range of velocities and the root-mean-square(RMS) amplitude is independent of the length. Jaap de Wilde (2005) [7] is the early researcher in the VIM study of Free standing Riser System (FRS) containing the Buoyancy Can. His investigation illustrates the components of FRS and set up a model test containing Buoyancy Can, cables, Riser, which demonstrate the relationship between vibration model and the current velocity, the trajectory of riser in X-Y plane. Due to the complexity of the model test system, Jaap de Wilde can only get some basic information about VIM phenomenon which has been observed by other researchers, which implied that complex systems to investigate some basic and simplified problem. To simplify the FRS and investigate the mechanical of VIM

phenomenon, Zhuang Kang et al. (2016) [1,2] present an experimental investigation on 6-DOF vortex-induced motion response of a tethered buoyancy can under conditions of different tether lengths and illustrate the relationship between the yaw motion and the motion in the inline and crossflow directions.

Numerical model is also an effective method to investigate the VIM issues, plenty of numerical tests have fit well with the experimental results in vortex induced motion of platform. Stéphane Etienne et al. (2010) [8] conduct two-dimensional numerical simulation to study the motion trajectory of cylinder after releasing the rotational degree of freedom. Minguez et al. (2012) [9-10] present a slender Buoyancy Can flow induced responses at high Re and 2D CFD model is built to investigate the yaw responses of the Buoyancy Can.

The aim of this paper is to presents 3D CFD model to analyse the flow induced response (FIR) especially the yaw motion of a Buoyancy Can and illustrate the relationship between the yaw motion and the motion in the inline and crossflow directions. Furthermore, the influence level of release in the degree of rotation is also illustrated in this paper.

2 NUMERICAL METHODS

2.1 Convention Equations

In this paper, a Delayed Detached-Eddy Simulation (DDES) method based on the Shear-Stress Transport (SST) model was used to simulate the turbulence detached flow during a large range of high Reynolds numbers [11-13]. SST-DDES is a hybrid Reynolds-Averaged Navier-Stokes (RANS) - Large Eddy Simulation (LES) method. It utilizes sub-grid scale model to handle the flow in the free shear flow area far away from the wall, and RANS's SST model is used to solve the flow in the boundary layer near the wall and other areas. This can guarantee the accuracy of LES solution, but also reduce the amount of calculation in the near-wall region of the boundary layer. For incompressible viscous fluids, the continuity equation and momentum equation can be expressed as:

$$\frac{\partial \overline{u}_i}{\partial x_i} = 0 \tag{1}$$

$$\frac{\partial \overline{u}_i}{\partial t} + \frac{\partial \overline{u}_j \overline{u}_i}{\partial x_j} = \frac{\partial \overline{P}}{\partial x_i} + \frac{\partial}{\partial x_j}\left[v\left(\frac{\partial \overline{u}_i}{\partial x_j} + \frac{\partial \overline{u}_j}{\partial x_i}\right)\right] - \frac{\partial \tau_{ij}}{\partial x_j} \tag{2}$$

Where v is the molecular viscosity, τ_{ij} is the Reynolds stress or sub-grid stress tensor. According to the Boussinesq hypothesis, τ_{ij} can be expressed as:

$$\tau_{ij} = \frac{2}{3}\delta_{ij}k - v_t\left(\frac{\partial \overline{u}_i}{\partial x_j} + \frac{\partial \overline{u}_j}{\partial x_i}\right) \tag{3}$$

SST-DDES turbulence model assumes that the turbulent viscosity v_t can be expressed as a function of turbulent kinetic energy k, turbulence dissipation rate ω and velocity strain S [14].

$$v_t = \frac{a_1 k}{\max(a_1\omega, SF_2)} \tag{4}$$

Where k and ω can be obtained by solving the corresponding transport equation:

$$\frac{\partial k}{\partial t} + \frac{\partial \left(u_j k\right)}{\partial x_j} = \tilde{G} - \frac{k^{\frac{2}{3}}}{l_{DDES}} + \frac{\partial}{\partial x_j}\left[\left(v + \alpha_k v_t\right)\frac{\partial k}{\partial x_j}\right] \tag{5}$$

$$\frac{\partial \omega}{\partial t} + \frac{\partial \left(u_j \omega\right)}{\partial x_j} = \gamma S^2 - \beta \omega^2 + \frac{\partial}{\partial x_j}\left[\left(v + \alpha_\omega v_t\right)\frac{\partial \omega}{\partial x_j}\right] - \left(1 - F_1\right)CD_{k\omega} \tag{6}$$

The l_{DDES} in equation (5) is the mixed length, which is the switch that controls the transformation between LES and RANS model [11].

2.2   Oversets Grid

Traditional dynamic grid method is difficult to deal with a large amplitude 6-Degrees-Of-Freedom (6-DOF) motion problem, and the oversets grid method is one of the effective ways to solve such problems. In this paper, oversets grid program Suggar ++ [15] is applied to calculate the Domain Connectivity Information (DCI). DCI mainly consists of cell information (hole cell, interpolated cell, donor cell, orphan cell) and interpolated weight coefficient. Naoe-FOAM-SJTU Solver [16-19] run OpenFOAM and Suggar ++ respectively in different processes to achieve full parallelization of the flow field solution and oversets grid digging interpolated calculation. Grid movement among different processes and DCI information exchange are through the Message Passing Interface (MPI). A detailed information concerning the coupling of OpenFOAM and Suggar ++ can be found in Shen's paper[20].

3   COMPUTATIONAL MODEL

3.1   Parameter Definition

In general, Buoyancy Can with 6-DOF under the constraint of the mooring system will induce significant surge, sway and yaw motions. In this paper, surge is assumed to be in-line with the flow, sway is the motion in transverse direction to the flow, and yaw is the rotation in z axis.

The characteristics of VIM are mainly determined by the reduced velocity U_r, the Reynolds number Re and the Strouhal number St, which are defined as:

$$U_r = \frac{U}{f_n D} \tag{7}$$

where U is the flow velocity, f_n is the natural frequency and D is diameter of the cylindrical Buoyancy Can.

$$\mathrm{Re} = \frac{UD}{v} \tag{8}$$

$$St = \frac{fD}{U} \tag{9}$$

where f is the vortex-shedding frequency. f is taken as the cross-flow frequency f_y. Similarly, U is the flow velocity, D is diameter of the cylindrical Buoyancy Can. and v is the fluid's kinematic viscosity coefficient.

The motion amplitude of the Buoyancy Can is expressed as dimensionless motion root-mean-square amplitude [1], defined as:

$$A_{RMS}^* = \frac{\sqrt{\frac{1}{N}\sum_{i=1}^{N}(x_i - \mu)^2}}{D} \qquad (10)$$

where x_i is the displacement of Buoyancy Can in a stable period, μ is the mean value of the displacement and D is diameter of the Buoyancy Can.

3.2 Computational Model

The computational model in this paper is the model in the towing experiment delivered by Zhuang Kang et al. (2016) [1]. The model of Buoyancy Can is in typical cylindrical shape and detail parameters of the Buoyancy Can are shown in Table 1.

Table 1: Parameters of the Buoyancy Can

Parameter	unit	value
D, outer diameter	mm	150
L, length	mm	700
△, Displacement	kg	12.37
w, weight	kg	4.24
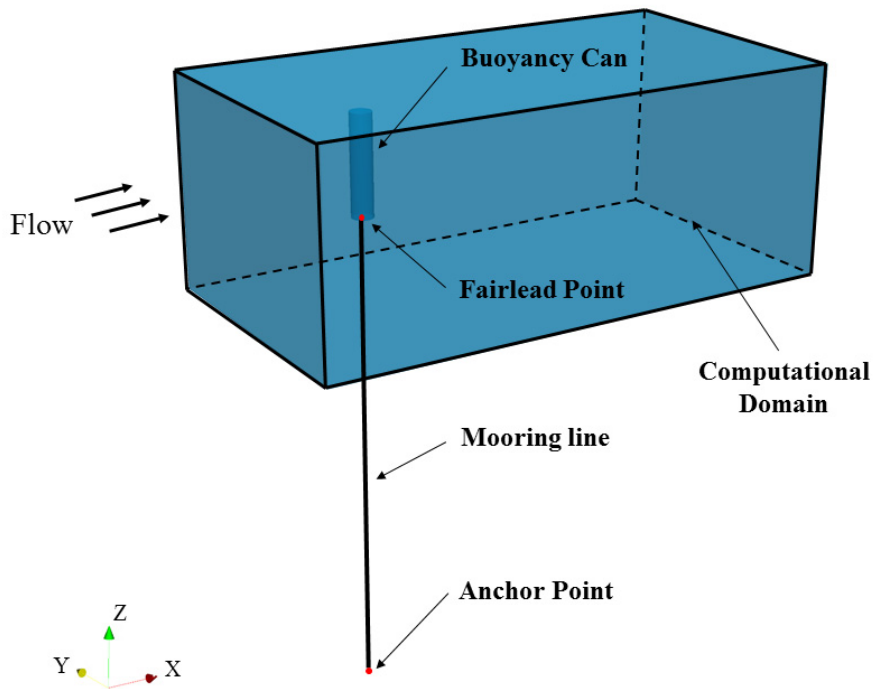
Figure 1: Schematic diagram of computational model

As shown in the Figure 1, the overall Buoyancy Can model is underwater regardless of the free surface issue. The Buoyancy Can is connected with a mooring line at the centre of the bottom of the model, fairlead point. And the anchor point is outside the computational domain.

3.3 Case Condition

In free decay test case, Buoyancy Can under no incoming flow is given an initial velocity of 0.2 m/s and released so that the model can be free to decay. While VIM test cases are carried out under uniform flow during a range of reduced velocities, from 4 to 10, and detail information is show in the following Table 2:

Table 2: VIM case condition

Reduced Velocity (Ur)	Flow Velocity/m·s^{-1}	Re
4	0.128	1.68×10^4
6	0.192	2.52×10^4
7	0.223	2.94×10^4
8	0.255	3.36×10^4
10	0.319	4.20×10^4

3.4 Computational Domain, Mesh, Boundary Condition
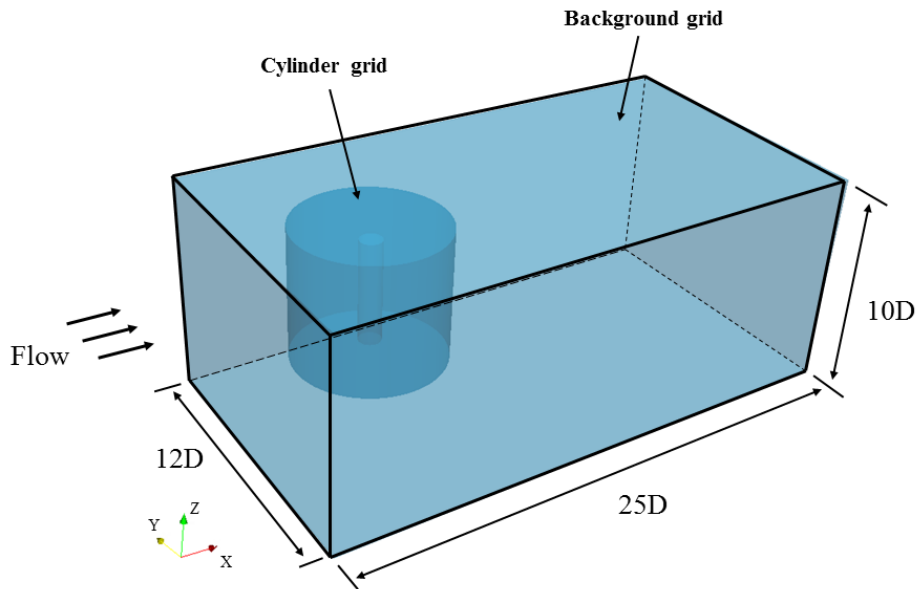
Figure 2: Computational domain
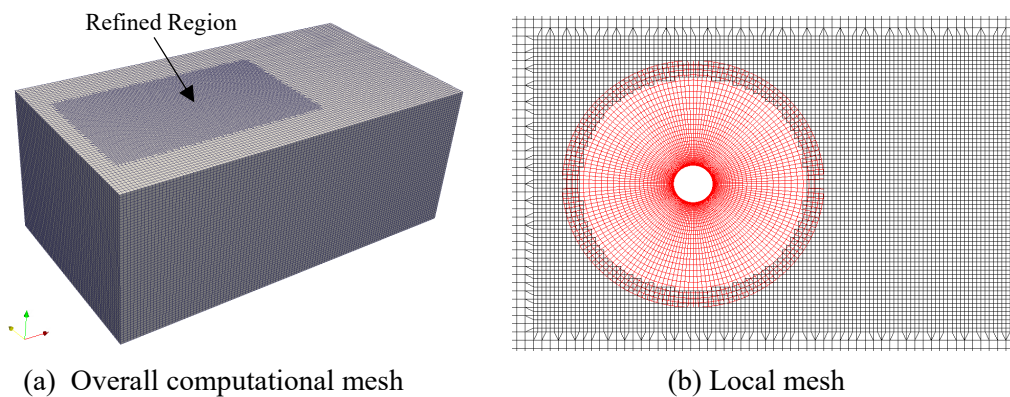
(a) Overall computational mesh   (b) Local mesh

Figure 3: Computational mesh

The computational domain and the mesh are shown in Figure 2 and 3. The length of the entire computational domain is 25D, the width is 12D, and the height is 10D. And the origin of the computational domain is set in the centre of the Buoyancy Can. The origin point is 5D from the upstream inlet, 20D from the downstream outlet, 6D from bottom face and 5D from side face.

Since the overset grid is applied in the cases, there are two kinds of mesh, one is cylinder grid, the other is background grid illustrated in Figure 3-(b). Both grids are structured grid and the vicinity of the cylinder is locally refined as the Figure 3-(a) shows. In cylinder grid region, the grid size near wall is set to small to obtain more accurate flow separation and y+ is about 5. And the grid number of background grid region is 0.71 million, while that of cylinder grid region is 1.62 million. Figure 3-(b) shows the local mesh distribution of cylinder at the z=0 section. The boundary conditions of the computational domain are set as follow: free stream velocity for inlet, pressure equals zero for outlet, symmetry for top, slip for other side patches.

4 RESULT AND DISCUSSION

4.1 Free Decay Test

In free decay test case, the Buoyancy Can under no incoming flow is given an initial velocity and released to get the natural period of the mooring system. Since the consecutive VIM numerical test is under the condition that the length of mooring line is 2.672m, the numerical free decay test keep the same length of mooring line. After the Fourier transform, it shows that the CFD result fit well with the Kang's experimental result [1] as Figure 4 present:

(a) Free decay profile   (b) Fourier transform profile
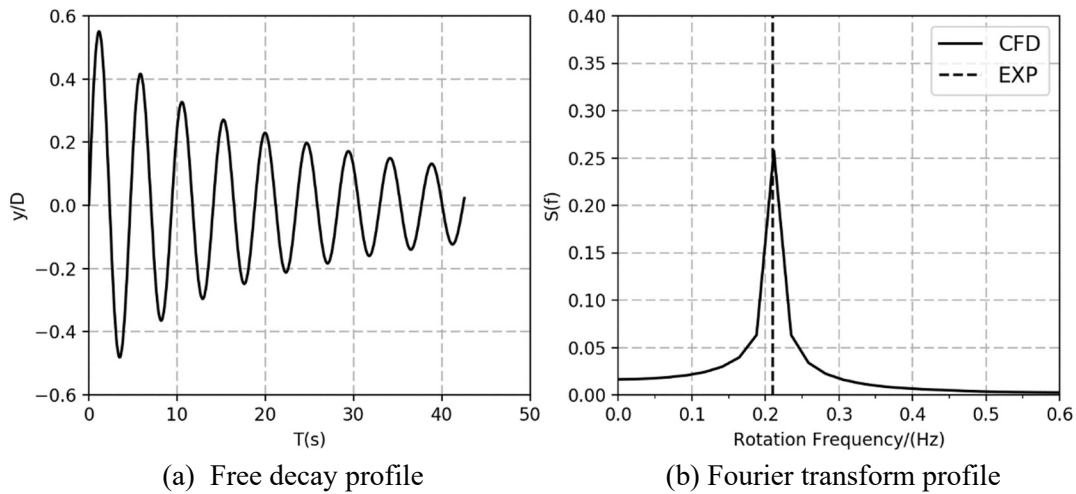
Figure 4: Tether length L=2.672m free decay result

4.2 Motion Trajectory

The VIM numerical test are delivered respectively at several reduced velocities (4/6/7/8/10), and Figure 5 present Time-Displacement profile, Fourier transform profile and Motion trajectory when reduced velocity equal to 4/6/8.
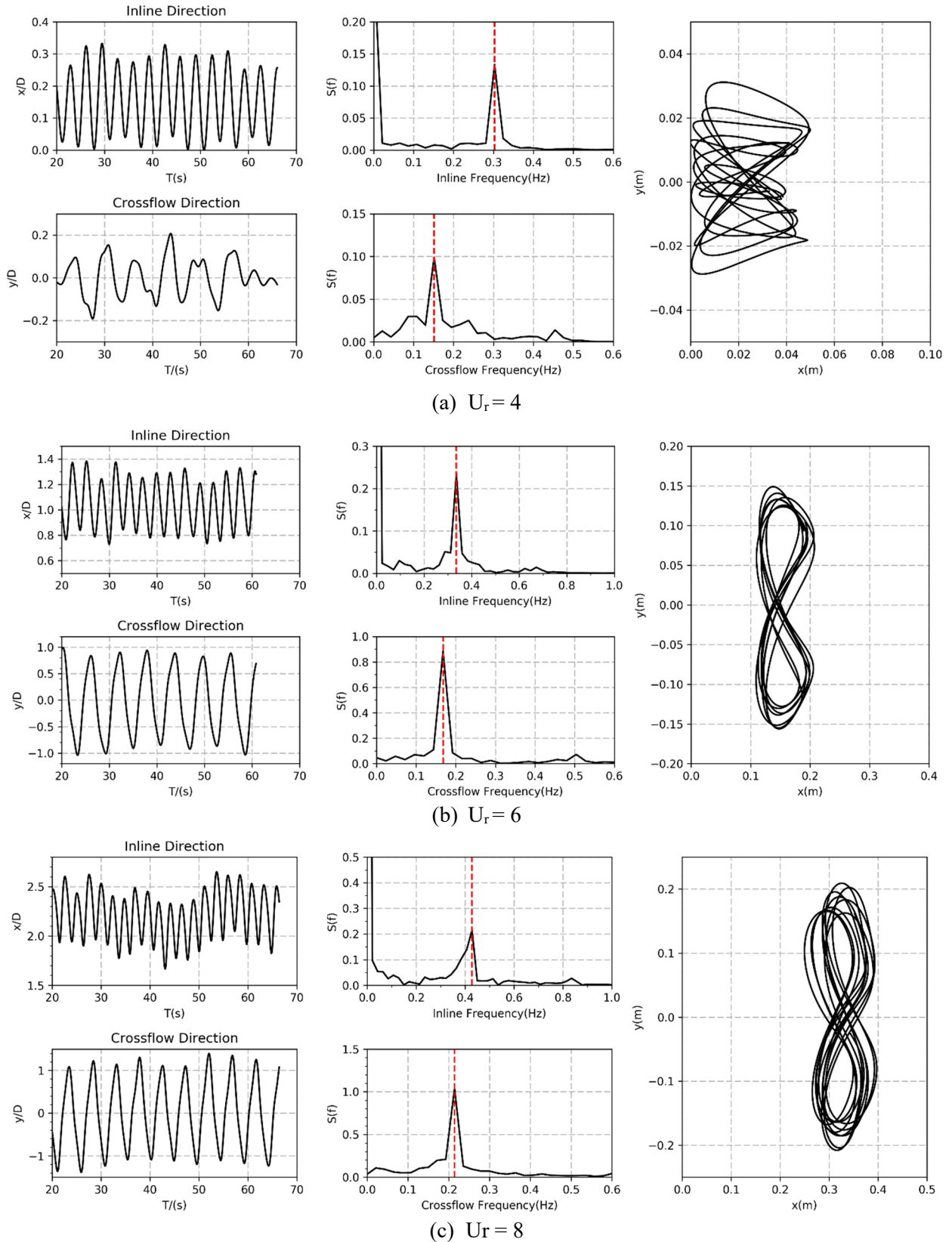
Figure 5: Time-Displacement profile & Fourier transform profile & Motion trajectory

As shown in Fig. 5, when reduced velocity is equal to 4, sway motion is unstable, and the amplitude of the sway frequency is approximate with the surrounding frequency peaks. Furthermore, with the increase of reduced velocity, the average surge displacement and surge and sway frequency of the Buoyancy Can is increased significantly. In general, when the vortex shedding is stable, the

motion trajectory becomes regular in "8" shape. The internal mechanism of the special shape is that the surge frequency is twice of the sway frequency just as Figure 6 present.
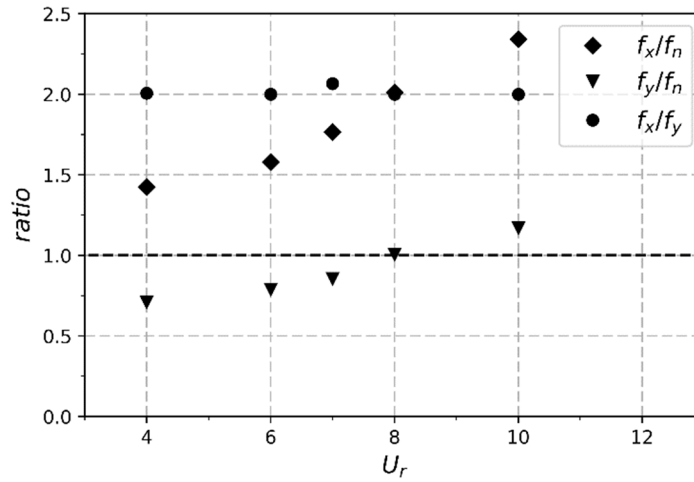
Figure 6: VIM frequency of the Buoyancy Can

Fig. 6 shows the trend of f_x/f_n, f_y/f_n, f_x/f_y of the cylinder versus reduced velocity U_r where f_n is the natural frequency, f_x is the surge frequency, f_y is the sway frequency. From the trend of these points, we can obtain that the ratio of the surge and the sway frequency is around 2 and the sway and surge frequency is increase with the reduced velocity, which is conform the VIM mechanism. In addition, "lock-in" phenomenon is not observed in these cases. The low mass ratio (mass ratio = 0.343) and only five cases in this paper may be the dominant reasons for this circumstance, and further studies should be delivered in this part.

4.3 Yaw Motion

(a) $U_r = 4$

(b) $U_r = 6$

(c) Ur = 8
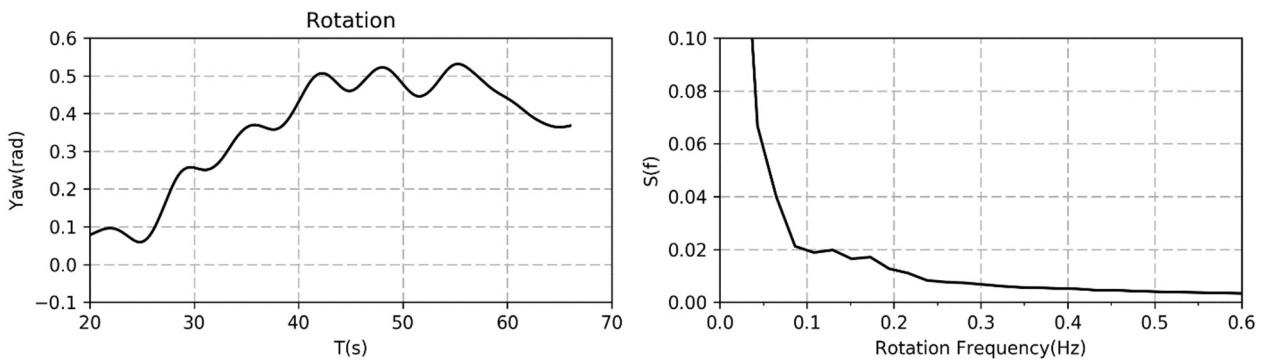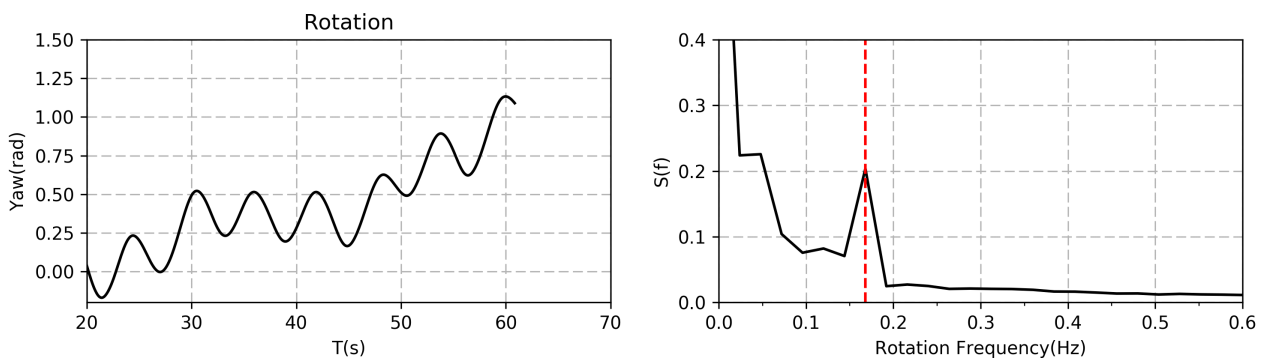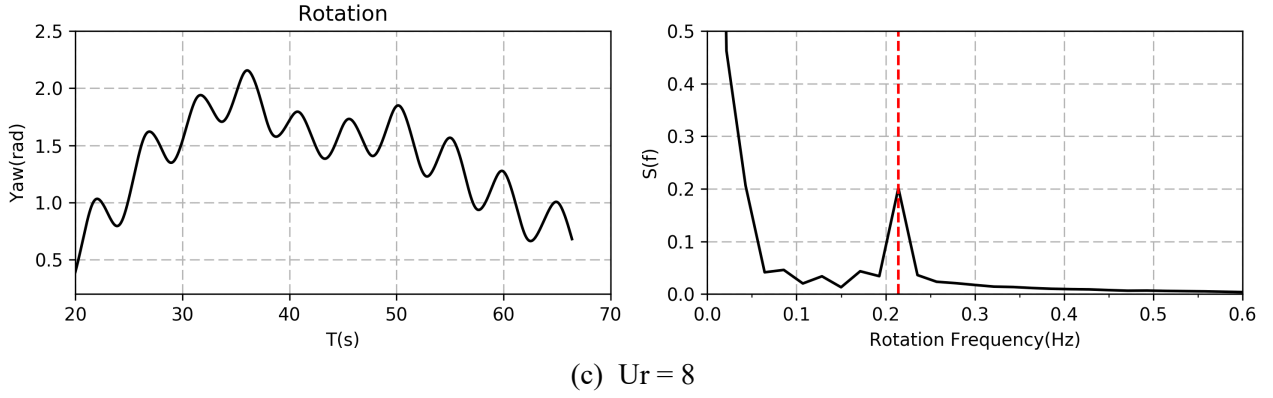
Figure 7: Time-Rotation profile & Fourier transform profile

In this paper, this numerical method can obviously capture the rotation phenomenon of the Buoyancy Can in the uniform flow. And the rotational frequency increases with the increase of the reduced velocity. From figure 7-(a), when the reduced velocity is low, we cannot tell the obvious dominant frequency in Fourier transform, which may cause by the unstable vortex shedding. When the vortex shedding is unstable, it is hard to form a stable moment to keep the cylinder rotate, so the dominant frequency cannot be observed in low reduced velocity.

Table 3: Surge frequency, Sway frequency and Yaw frequency

Reduced Velocity (Ur)	Surge frequency/Hz	Sway frequency/Hz	Yaw frequency/Hz
4	0.303	0.151	-
6	0.336	0.168	0.168
7	0.376	0.182	0.182
8	0.428	0.214	0.214
10	0.498	0.249	0.249

According to the Table 3, the same with surge and sway frequency, the yaw frequency increases with the increase of reduced velocity. Secondly, yaw frequency is equal to the sway frequency, which is consistent with Kang's experimental result [1]. The reason for this circumstance is that the sway motion and yaw motion are both caused by the vortex shedding. And we can conjecture that the sway motion and yaw motion share the same exciting force component.

After that, we carried out two cases, one fixed in rotation and the other one free in rotation when reduced velocity equal to 7.
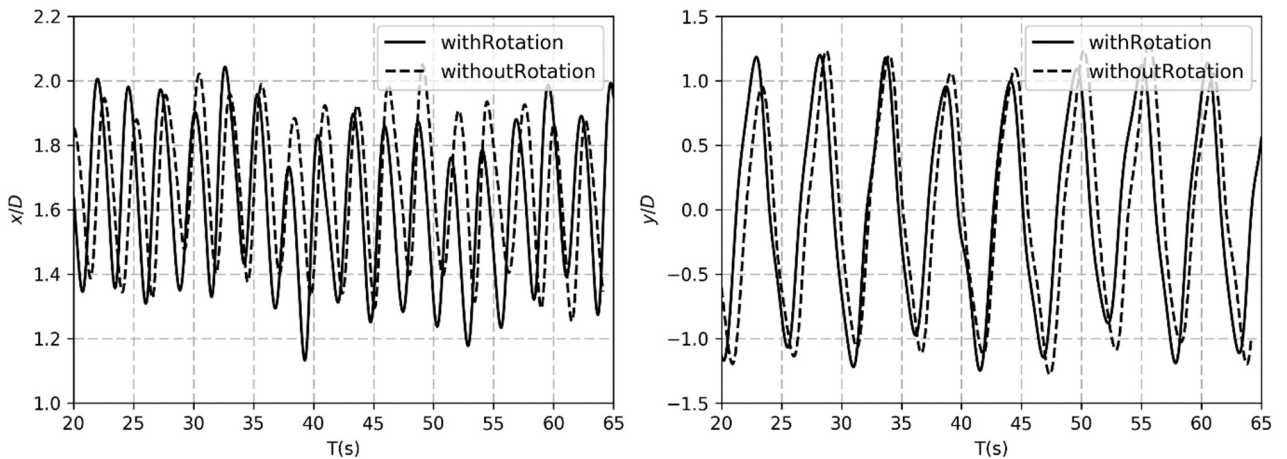
Figure 8: Dimensionless sway and surge amplitude in time series

In Figure 8, whether release the degree of rotation show few difference in time series profile, but it indicates that the release in degrees of rotation induces the Buoyancy Can obtain the stable vortex shedding slightly earlier. Furthermore, the RMS of the surge and sway motion amplitudes are calculated in Table 4.

Table 4: Surge and sway amplitude RMS in Ur=7

Case	Rotation	Without Rotation
Surge Amplitude RMS	0.218	0.215
Sway Amplitude RMS	0.747	0.765

In Table 4, it indicates that release in the degree of rotation can decrease the sway amplitude, while this change makes no difference in the surge amplitude, which is conform the two dimensional numerical result of Stéphane Etienne et al [8]. But in his work, the decrease in sway motion is more obvious than that of our work. The reason for this difference may be that three dimensional flow much more complicated than the two dimensional flow and the vortex shedding in free end of the Buoyancy Can may affect the rotation motion.

5 CONCLUSION

This paper presents 3D CFD simulation to analyse the flow induced response (FIR) especially the yaw motion of a Buoyancy Can. The numerical tests are conducted with a Buoyancy Can under different reduced velocities utilizing naoe-FOAM-SJTU including SST-DDES model and oversets grid method. And the following conclusions are made:

1. The numerical model in this paper can predict the free decay test and VIM test well with the experiment. And in VIM cases, with the increase of the reduced velocity, the stable vortex shedding can be observed in result and the motion trajectory becomes regular in "8" shape.

2. The yaw frequency increases with the increase of reduced velocity, which is similar with surge and sway frequency. And yaw frequency is equal to the sway frequency, which imply that the sway motion and yaw motion share the same exciting force component.

3. In the state of Reynolds number equal to 2.94×104, the rotational degree of freedom in Buoyancy Can can slightly decrease the RMS of sway amplitude in 2.41% but make no difference to the RMS of surge amplitude.

The future work includes the study in the influence of rotating damping and the mechanism of vortex induced rotation. And in this paper Reynolds number is around 10^4, high Reynolds numerical test will also be set in the future work.

REFERENCES

1. Zhuang Kang, Wenchi Ni, Gang Ma, Xiang Xu (2017). A model test investigation on vortex-induced motions of a buoyancy can. *Marine Structures*, 53, 86-104.

2. Zhuang Kang, Wenchi Ni, Xu Zhang, Liping Sun (2016). An Experimental Investigation of Six-Degrees-of-Freedom VIM characteristics of a tethered buoyancy can. *Proceedings of the Twenty-sixth (2016) International Ocean and Polar Engineering Conference*, Rhodes, Greece.

3. Daniel Karunakaran, Dan Lee and John Mair, Subsea 7 (2009). Qualification of the Grouped SLOR Riser System. *The 2009 Offshore Technology Conference*, Houston, Texas, USA.

4. Irani Mehernosh, Finn Lyle (2004). Model testing for vortex induced motions of spar platforms. *Proceedings of the 23rd International Conference on Offshore Mechanics and Arctic Engineering*, Vancouver, BC, Canada, OMAE.

5. Oakley Jr. Owen H., Navarro Claudia, Constantinides Yiannis, and Holmes Samuel (2005). Modeling vortex induced motions of spars in uniform and stratified flows. *Proceedings of the 24th International Conference on Off shore Mechanics and Arctic Engineering*, Halkidiki, Greece, OMAE, 885-894

6. Govardhan R, Williamson CHK (1997). Vortex-induced motions of a tethered sphere. *Journal of Wind Engineering and Industrial Aerodynamics*, 69-71, 375-85.

7. Jaap de Wilde (2007). Model tests on the Vortex Induced Motions of the Air Can of a Free Standing Riser System in Current, *Proceedings of the Deep Offshore Technology Conference*, October 10th-12th, Stavanger, Norway.

8. Stéphane Etienne, Emmanuel Fontaine (2010). Effect of the rotational Degree of Freedom on Vortex-Induced Vibrations of a circular cylinder in Cross-Flow. *Proceedings of the 20th International Offshore and Polar Engineering Conference*, Beijing, China, June 20-25.

9. Minguez, Ange Luppi,Anthony Berger (2012). Slender Buoy FSHR Vortex Induced Rotations. *Proceedings of the ASME 31th International Conference on Ocean*, Offshore and Arctic Engineering, Rio de Janeiro, Brazil.

10. Minguez, Ange Luppi, Stephane Pattedoie, Rene Maloberti (2011). Slender Buoy VIM & VIR Analysis by CFD/FSI Approach. *Proceedings of the ASME 30th International Conference on Ocean, Offshore and Arctic Engineering*, Rotterdam, The Netherlands.

11. Weiwen Zhao, Decheng Wan (2016). Detached-Eddy Simulation of Flow Past Tandem Cylinders. *Applied Mathematics and Mechanics*, 37(12): 1272-1281

12. Weiwen Zhao, Decheng Wan (2016). Numerical Study of 3D Flow past a Circular Cylinder at Subcritical Reynolds Number Using SST-DES and SST-URANS. *Chinese J Hydrodynamics*, 31(1), 1-8.

13. Zhenghao Liu, Weiwen Zhao, Decheng Wan (2017). Numerical Simulation of Vortex-Induced Motion of a Deep Draft Semi-Submersible Platform. *The 27th International Ocean and Polar Engineering Conference*, San Francisco, CA, USA.

14. Menter F R, Kuntz M, Langtry R (2003). Ten years of industrial experience with the SST turbulence model. *Turbulence, Heat and Mass Transfer*. 4(1): 625–632.

15. Noack R W, Boger D A, Kunz R F (2009). Suggar++: An improved general overset grid assembly capability. *19th AIAA Computational Fluid Dynamics Conference*. San Antonio, Texas, USA.

16. Zhirong Shen, Decheng Wan (2012). The manual of CFD solver for ship and ocean engineering flows: naoe-FOAM-SJTU. Shanghai, China, Shanghai Jiao Tong University.

17. Zhirong Shen, Decheng Wan (2013). RANS computations of added resistance and motions of a ship in head waves. *International Journal of Offshore and Polar Engineering*. 23(4): 263–271.

18. Jianhua Wang, Xiaojian Liu and Decheng Wan (2015). Numerical Simulation of an Oblique Towed Ship by naoe-FOAM-SJTU Solver, Proceedings of the Twenty-fifth (2015) International Ocean and Polar Engineering Conference (ISOPE), Kona, Big Island, Hawaii, USA.

19. Jianhua Wang , Xiaojian Liu, Decheng Wan, Gang Chen (2016). Numerical Prediction of KCS Self-Propulsion in Shallow Water. Proceedings of the Twenty-sixth International Ocean and Polar Engineering Conference, Rhodes, Greece.

20. Zhirong Shen, Decheng Wan and Pablo Carrica (2015). Dynamic overset grids in OpenFOAM with application to KCS self-propulsion and maneuvering. *Ocean Engineering*. 108: 287–306.